The Canadian Mineralogist
Vol. 58, pp. 381-394 (2020)
DOI: 10.3749/canmin.2000003

BADAKHSHANITE-(Y), $Y_2Mn_4Al(Si_2B_7BeO_{24})$, A NEW MINERAL SPECIES OF THE PERETTIITE GROUP FROM A GRANITE MIAROLIC PEGMATITE IN EASTERN PAMIR, THE GORNO BADAKHSHAN AUTONOMOUS OBLAST, TAJIKISTAN

Leonid A. PAUTOV

A.E. Fersman Mineralogical Museum, Russian Academy of Sciences, Leninskii Prospekt 18-2, Moscow 117071, Russia
Institute of Minerology UB RAS, Miass, Chelyabinsk district, 456317, Russia

Mirak A. MIRAKOV

Institute of Geology, Earthquake Engineering and Seismology, Academy of Sciences,
Aini ul. 267, 734063, Dushanbe, Tadzhikistan

Fernando CÁMARA[§]

Dipartimento di Scienze della Terra, Università di Torino, I-10125, Torino, Italy
CrisDi - Interdepartmental Center for Crystallography, via Giuria 7, 10126, Torino, Italy

Elena SOKOLOVA and Frank C. HAWTHORNE

Department of Geological Sciences, 125 Dysart Road, University of Manitoba, Winnipeg, Manitoba, R3T 2N2, Canada

Manuchekhr A. SCHODIBEKOV

Institute of Geology, Earthquake Engineering and Seismology, Academy of Sciences,
Aini ul. 267, 734063, Dushanbe, Tadzhikistan

Vladimir Yu. KARPENKO

A.E. Fersman Mineralogical Museum, Russian Academy of Sciences, Leninskii Prospekt 18-2, Moscow 117071, Russia

Abstract

Badakhshanite-(Y), ideally $Y_2Mn_4Al(Si_2B_7BeO_{24})$, is a tetrahedral sheet-structure mineral found in the Dorozhny (Road) miarolitic granitic pegmatite within the Kukurt pegmatite field 45 km E of Murghab, Eastern Pamir, Gorno-Badakhshan Autonomous Oblast, Tajikistan. Badakhshanite-(Y) occurs in medium- to coarse-grained non-graphic albite-microcline-quartz pegmatites in close association with smoky quartz, Sc-bearing spessartine, Sc-bearing tusionite, and schorl. It often grows together with Sc-bearing tusionite and occurs as single columnar crystals ranging from 50 to 400 μm in length, as inclusions in spessartine and tourmaline, and rarely as crystals in blebs along boundaries between garnet, tourmaline, and quartz. Badakhshanite-(Y) is yellow brown and has a white streak and a vitreous luster. It is brittle, with a conchoidal fracture, Mohs hardness of 6.5–7, and calculated density of 4.41 g/cm. In thin section it is transparent and pale yellow, non-pleochroic, biaxial (–), with $\alpha = 1.805(2)$, $\beta_{calc} = 1.827$, $\gamma = 1.835(3)$ ($\lambda = 590$ nm); $2V$ (meas.) = –60(10)°. Dispersion is weak, $r > v$. Extinction is straight, elongation is negative. FTIR spectra show the absence of (OH) and H_2O groups. Chemical analysis by electron microprobe using WDS (6 points), SIMS, and ICP-OES for B and Be gave SiO_2 11.96, ThO_2 0.12, Sm_2O_3 0.17, Gd_2O_3 0.30, Tb_2O_3 0.10, Dy_2O_3 0.73, Ho_2O_3 0.19, Er_2O_3 1.34, Tm_2O_3 0.54, Yb_2O_3 8.82, Lu_2O_3 2.32, Y_2O_3 16.60, Sc_2O_3 1.57, Al_2O_3 3.06, B_2O_3 22.06, FeO 0.94, MnO 23.33, CaO 0.58, BeO 2.84, total 97.57 wt.%.The empirical formula based on 24 O *apfu* is $(Y_{1.21}\mathit{REE}_{0.78}Th_{0.01})_{\Sigma 2}(Mn_{3.47}Y_{0.34}Ca_{0.11}Fe^{2+}{}_{0.08})_{\Sigma 4}(Al_{0.63}Sc_{0.24}Fe^{2+}{}_{0.06}\square_{0.07})_{\Sigma 1}[(Si_{2.10}B_{6.69}Be_{1.20})_{\Sigma 9.99}O_{24}]$, where $\mathit{REE} = (Yb_{0.47}Lu_{0.12}Dy_{0.04}Er_{0.07}Tm_{0.03}\ Ho_{0.01}Gd_{0.02}Sm_{0.01}Tb_{0.01})_{\Sigma 0.78}$. Badakhshanite-(Y) is orthorhombic, space group *Pnma*, *a* 12.852(1), *b* 4.5848(5), *c* 12.8539(8) Å, *V* 757.38(7) Å^3, $Z = 2$. The crystal structure was refined to $R_1 = 4.31\%$ based on 1431

[§] *Corresponding author e-mail address*: fernando.camara@unimi.it

unique [$F > 4\sigma F$] reflections. In the crystal structure of badakhshanite-(Y), a layer of tetrahedra parallel to (010) is composed of four different tetrahedrally coordinated sites: *Si*, *B*(1), *B*(2), and *T* ($\langle$Si–O$\rangle$ = 1.623 Å, $\langle$B(1)–O$\rangle$ = 1.485 Å, $\langle$B(2)–O$\rangle$ = 1.479 Å, $\langle$T–O$\rangle$ = 1.557 Å), which form four-, five-, and eight-membered rings, having the composition ($Si_2B_7BeO_{24}$). Between the sheets of tetrahedra, there are three cation sites: *M*(1), *M*(2), and *M*(3) ($\langle$M(1)–O$\rangle$ = 2.346 Å, $\langle$M(2)–O$\rangle$ = 2.356 Å, $\langle$M(3)–O$\rangle$ = 2.016 Å) occupied by Y(*REE*), Mn^{2+}(Y, Ca, Fe^{2+}), and Al(Sc), respectively. The *M*(1,2) sites ideally give Y_2Mn_4 *apfu*; the *M*(3) site ideally gives Al *apfu*. Badakhshanite-(Y) is an Al- and Be-analogue of perettiite-(Y).

Keywords: Badakhshanite-(Y), new mineral, crystal structure, chemical formula, Kukurt pegmatite field, Gorno-Badakhshanskij Autonomous Region, Republic of Tajikistan.

Introduction

Badakhshanite-(Y) is a new mineral found in the miarolitic Dorozhny (Road) granitic pegmatite in the Kukurt pegmatite field, Eastern Pamir, Gorno-Badakhshan Autonomous Oblast, Tajikistan. Badakhshanite-(Y), ideally $Y_2Mn_4Al(Si_2B_7BeO_{24})$, is an Al- and Be-analogue of perettiite-(Y), ideally $Y_2Mn_4Fe^{2+}(Si_2B_8O_{24})$ (Danisi *et al.* 2015) and is related to perettiite-(Y) by the substitution $^{M(3)}Al^{3+} + {}^{T}Be^{2+} \leftrightarrow {}^{M(3)}Fe^{2+} + {}^{T}B^{3+}$. Badakhshanite-(Y) [бадахшанит-(Y)] is named for its type locality. The new mineral and its name have been approved by the IMA Commission on New Minerals, Nomenclature and Classification (IMA no. 2018-085). The holotype specimen has been deposited in the collections of the Fersman Mineralogical Museum of the Russian Academy of Sciences, Moscow, Russia, registration number # 5235/1.

Occurrence and Paragenesis

The mineral occurs in the Dorozhniy miarolitic granite pegmatite within the Kukurt pegmatite field, 45 km E of Murghab, Eastern Pamir, Gorno-Badakhshan Autonomous Oblast, Tajikistan (Fig. 1). The pegmatite field lies within the Muzkol-Rangkulsky anticlinorium, in the core of which a ledge of Precambrian basement is exposed. The pegmatites are related to leucocratic binary granites of the Shatputsky complex of Alpine age (Dmitriev 1983, Rossovsky *et al.* 1991). The Dorozhny pegmatite is a series of high-angle pulled-together pegmatite veins with an exposed length of about 100 m and a width of up to 10–15 m (Fig. 2); it is limited to a curved section of the Kukurt anticline (Rossovsky *et al.* 1991, Skrigitil' 1996). The host rocks are amphibolite and epidote-amphibolite facies slates and marbles of the Sarydzhilga series (Neoproterozoic (?) age). There is a zonal structure in the wider parts of the pegmatite: a core of greyish-white quartz underlain by a zone of graphic pegmatite. In 1982, a miarolitic cavity 60 × 180 × 60 cm with large crystals of smoky quartz ("morion"), fluorite, a polychromic elbaite, and hambergite was discovered in a bulge of the central part of the vein (Rossovsky *et al.* 1991, Dzhurayev *et al.* 1998, Zolotarev 1996). Rock-forming minerals of the pegmatite are as follows: quartz, microcline, "oligoclase", schorl, and spessartine (sometimes Sc-bearing) (Mirakov *et al.* 2018a); minor minerals are muscovite and albite. Common accessory minerals are columbite-(Mn), thorite, zircon, monazite-(Ce), cassiterite, magnetite, fluorapatite, fluorite, beryl, titanite, and rutile; rare accessory minerals are scheelite and hambergite (Dzhurayev *et al.* 1998), Sc-bearing tusionite (Mirakov *et al.* 2018b), high-B crystalline gadolinite, uranopolycrase, allanite-(Ce), thorianite, uraninite, herzenbergite, xenotime-(Y), ilmenite, hematite, helvine, bismutocolumbite, a Sc-tantalate, and a Cs-mica currently under investigation.

Badakhshanite-(Y) occurs in a medium- to coarse-grained non-graphic albite-microcline-quartz pegmatite with schorl and Sc-bearing spessartine. Badakhshanite-(Y) often grows together with Sc-bearing tusionite (Fig. 3). Badakhshanite-(Y) occurs as single columnar crystals, from 50 to 400 μm in length (average size in largest dimension is 150 μm), included in spessartite and tourmaline (Fig. 3), and rarely occurs as crystals in blebs along boundaries of garnet with tourmaline and quartz. Some crystals show skeletal growth.

Physical and Optical Properties

Badakhshante-(Y) is yellow-brown in color, has a white streak and vitreous luster. It is brittle with a conchoidal fracture. In BSE mode and transmitted light (Fig. 4), slight sector-growth zoning and "hourglass" textures occur in sections of badakhshanite-(Y) crystals. Mohs hardness is 6.5–7. The hardness, obtained by micro-indentation tests, is $VHN_{100-200}$ = 947 kg/mm (variation on four measurements is 784–1160). Neither cleavage nor parting is observed. Measured density is more than 4.27(2) g/cm^3 (it settled in Clerici liquid). Density calculated using the empirical formula is 4.41 g/cm^3, and 4.25 g/cm^3 using the ideal formula. The mineral does not fluoresce in short- or long-wave ultraviolet light. In thin section, it

FIG. 1. A schematic map of Tajikistan, showing the location of the Kukurt pegmatite field, East Pamir (red square).

is pale yellow and transparent. The fine twinning in badakhshanite-(Y), like that described for perettiite-(Y) (Danisi *et al*. 2015), makes detailed optical characterization of the mineral impossible. The conoscopic figure, obtained from extremely small areas, is clearly biaxial negative, but the estimated $2V$ angle is approximate because of diffuse isogyres. Axial dispersion is not observed. Only α and γ were measured because of the twinning. Badakhshanite-(Y) is biaxial (–) with $\alpha = 1.805(2)$, $\beta_{\text{calc}} = 1.827$, $\gamma = 1.835(3)$ (λ = 590 nm); $2V$ (meas.) = –60(10)°. Dispersion is weak, $r > v$. Extinction is straight, elongation is negative. Pleochroism is not observed.

FTIR SPECTROSCOPY

A spectrum was obtained in the range 400–4000 cm^{-1} from badakhshanite-(Y) powder mixed with dried KBr and pelletized, using a Shimadzu IR-Fourier spectrometer with a resolution of 2 cm^{-1} and 100 scans (Fig. 5). The IR spectrum of an analogous pellet of pure KBr was used for comparison, and there are weak bands in the spectrum which probably correspond to H_2O absorbed by the KBr pellet. An additional IR

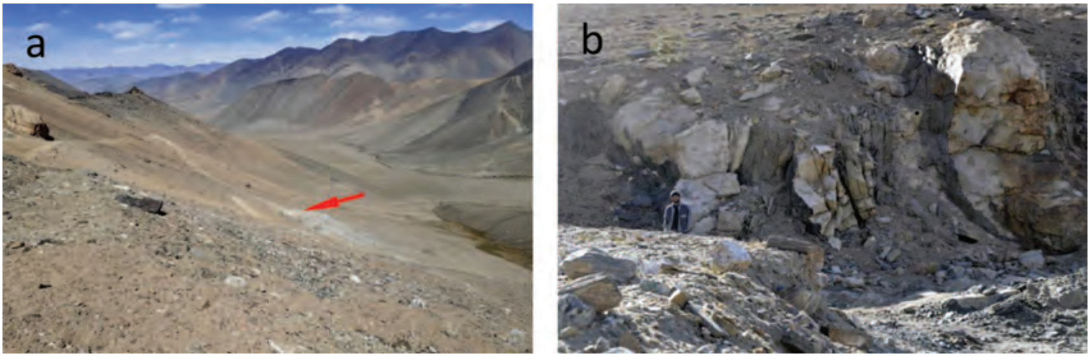

FIG. 2. The Kukurt pegmatite field, East Pamir. (a) View of the valley of the Kukurt river. The red arrow points to the Dorozhny pegmatite. (b) A view of the Dorozhny pegmatite in the wall of a small open cut on the left side of the Kukurt valley (photo from 2018).

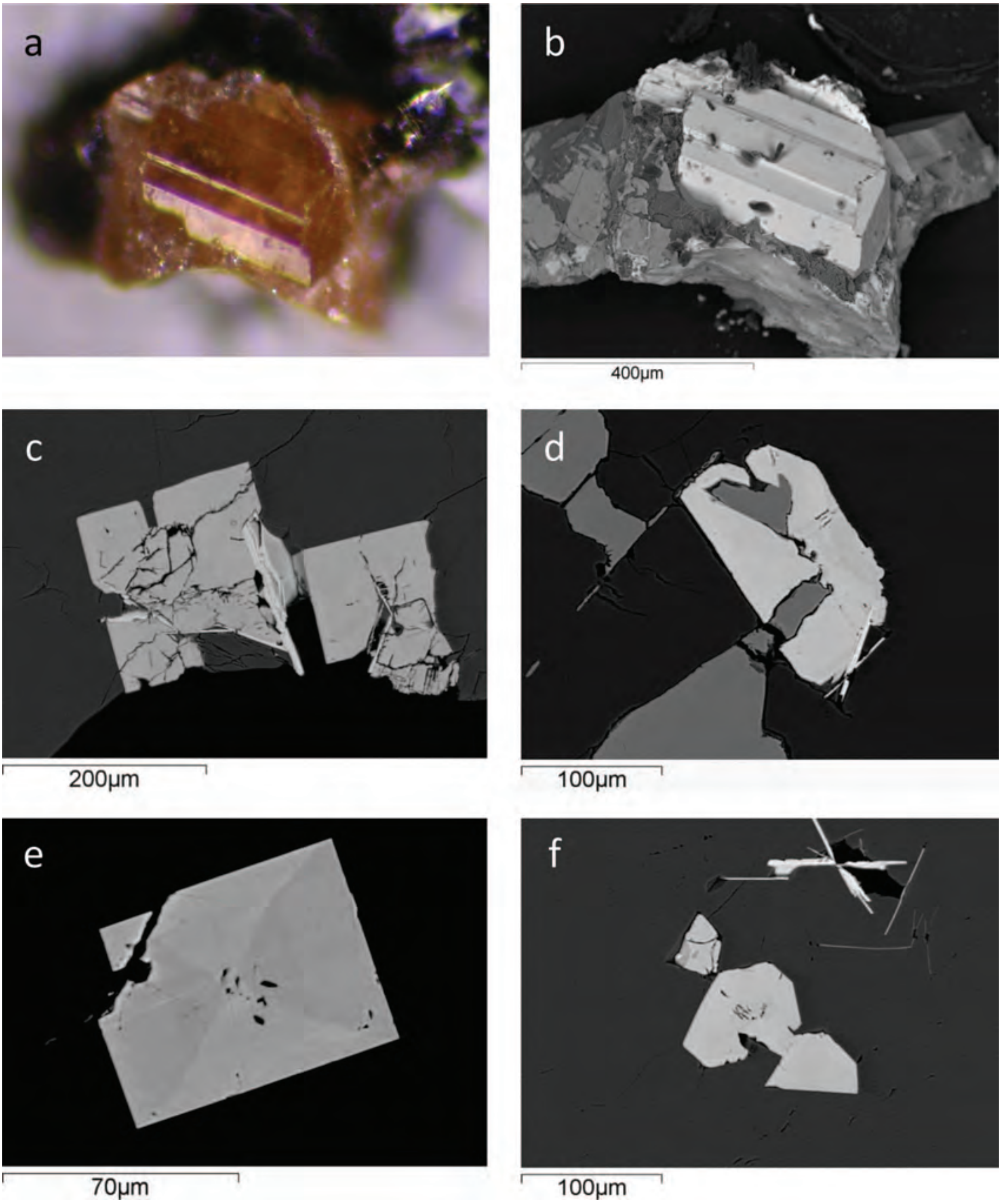

FIG. 3. (a, b) Badakhshanite-(Y) crystals on spessartine and quartz aggregate: in oblique light under a binocular microscope (a), and in BSE mode (b). (c–f) Badakhshanite-(Y) crystals in polished sections; lamellar white – Sc-bearing tusionite, light grey – badakhshanite-(Y), grey – spessartine, dark grey – tourmaline. BSE image.

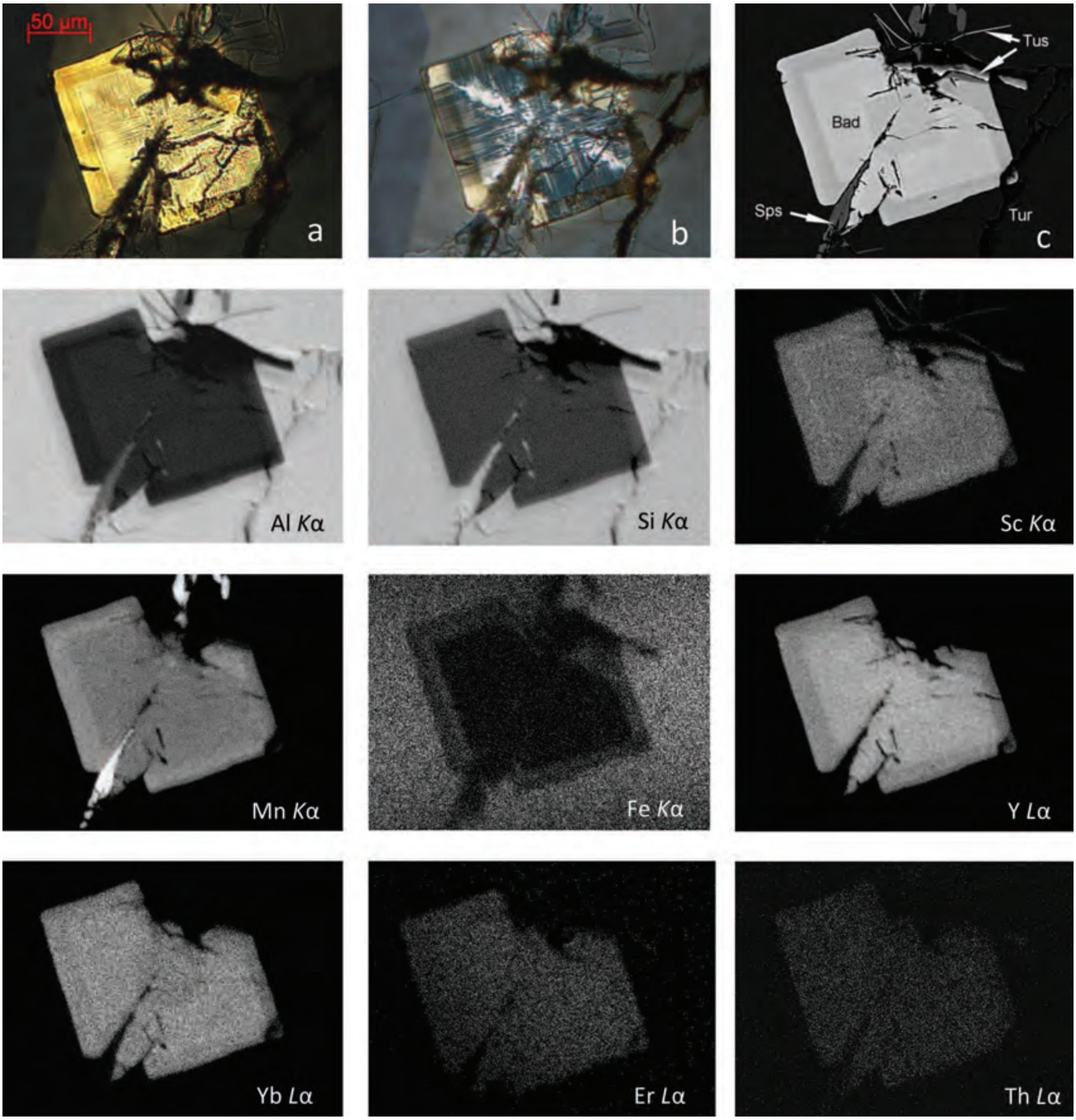

FIG. 4. Cross section through a badakhshanite-(Y) crystal. View in transmitted light with (a) one polarizer, (b) with crossed polarizers, (c) the same area of the section in BSE mode, and characteristic X-ray radiation of the elements, specified under the pictures. Bad – badakhshanite-(Y), Tur – tourmaline, Sps – spessartine, Tus – tusionite.

spectrum in the range 400–1600 cm^{-1} was obtained from another KBr pellet with badakhshanite-(Y), using a Specord 75-IR spectrometer.

Bands in the range 900 to 1200 cm^{-1} correspond to T–O stretching vibrations (T = Si, B). Absorptions in the 750–900 cm^{-1} range are due to Be–O stretching vibrations. The lines at 643 and 593 cm^{-1} are attributed to O–T–O bending vibrations. The absorption at 530–560 cm^{-1} belongs to Al–O stretching vibrations. The 449 cm^{-1} feature can be related to T–O–T deformational vibrations.

CHEMICAL COMPOSITION

The chemical composition of badakhshanite-(Y) was measured using electron probe microanalysis and ICP-OES analysis in the laboratory of the A.E. Fersman Mineralogical Museum of the RAS (Moscow, Russia) and SIMS at the Institute of Microelectronics and Informatics of the RAS (Yaroslavl', Russia). Microprobe analysis was done using a JEOL Superprobe 733 in both EDS and WDS modes. Analyses obtained on both types of spectrometers agree well. The EDS analyses were done with a Si(Li)-detector and an INCA Energy 350 (Oxford) analysis system at 20 kV, probe current 1 nA, probe diameter 1–5 μm. Standards used were as follows [element(analytical line) – standard]: Mg($K\alpha$) – diopside; Si($K\alpha$) – quartz; Al($K\alpha$) – kyanite; Mn($K\alpha$) – $MnTiO_3$; Fe($K\alpha$) – Fe_2O_3; Ca($K\alpha$) – diopside; Sc($K\alpha$) – Sc_2O_3; Th($M\alpha$) – ThO_2; U($M\alpha$) – UO_2; Y($L\alpha$) – Y_2O_3; Dy($L\alpha$) – Dy_2O_3; Ho($L\alpha$) – Ho_2O_3; Er($L\alpha$) – Er_2O_3; Yb($L\alpha$), Gd($L\alpha$), Sm($L\alpha$), Tm($L\alpha$), Tb($L\alpha$), and Lu($L\alpha$) – synthetic single-element phosphates (*REE*PO_4). The WDS analyses (except boron) were done with an accelerating voltage of 20 kV, a beam current of 20 nA, and a beam diameter of 1–5 μm. Count times at peaks were 20 s and at backgrounds were 10 s for Si, Al, Mn, Yb. For the other elements: 80 s at peak, 40 s at background. Standards used were as follows: Mg($K\alpha$), Si($K\alpha$), Al($K\alpha$), Fe($K\alpha$), and Ca($K\alpha$) – pyrope USNM 143968; Mn($K\alpha$) – $Mn_{1.97}Mg_{0.03}SiO_4$; Sc($K\alpha$) – Sc_2O_3; Th($M\alpha$) – ThO_2; U($M\beta$) – UO_2; Y($L\alpha$) – Y_2O_3; Dy($L\beta$) – Dy_2O_3; Ho($L\beta$) – Ho_2O_3; Er($L\alpha$) – Er_2O_3; Tb($L\alpha$) – TbF_3; Yb($L\alpha$), Gd($L\alpha$), Sm($L\alpha$), Tm($L\alpha$), and Lu($L\alpha$) – synthetic single-element phosphates (*REE*PO_4). For WDS mode for B_2O_3, the accelerating voltage was 5 kV, beam current 100 nA, beam diameter 20 μm, the intensity was estimated from the peak area, and the standard used was danburite. Lanthanum, Ce, and Nd were searched for but not found. Detection limits were ~500 ppm for Y, U, and Th and 1000 ppm for *REE*. Manganese, Dy, and Th peak overlaps on Dy, Yb, and U, respectively, were corrected. The data were reduced and corrected by the PAP method of Pouchou & Pichoir (1985).

Ion probe measurements were done with a Cameca IMS 4F ion microprobe (analyst S.G. Simakin). An O_2^- primary beam was used instead of O^- that is commonly used. The use of molecular *versus* atomic oxygen ions has the advantage of lower transient depth and thickness of the altered layer and a twice-lower charge carried by the bombarding ions for the same sputtering rate. This choice can improve sensitivity and accuracy of the analyses. Absolute concentrations for each element were calculated from the ion-current ratio element/$^{30}Si^+$ using calibration constants from the following reference samples: Li – spodumene, B – danburite, Be – phenakite.

Inductively coupled plasma-optical emission spectrometry (ICP-OES) was done with a Varian 720-ES parallel optical spectrometer. A badakhshanite-(Y) crystal was fused in a Pt crucible with high-purity Na_2CO_3. The resultant fusion cake was dissolved in a solution of HNO_3 at 2% concentration. The acids used were purified by double distillation without boiling. The resistivity of water used for the solutions was 18.2 MΩ/cm; calibration solutions were prepared from multi-element standard solutions of Merk. Secondary ion mass spectrometry (SIMS) and ICP-OES analysis of badakhshanite-(Y) gave traces of Li (wt.%), 0.003 and <0.005 respectively, much lower than the Li contents reported for perettiite-(Y) (Danisi *et al.* 2015).

X-ray fluorescence analyses show that Fe is very low, and Al and Sc are significant. Growth zonation and sector zoning in badakhshanite-(Y) crystals were observed both in thin sections and in BSE mode and are related to small variations in Mn, Fe, Sc, Y, and *REE* contents (Fig. 4). The absence of H_2O and CO_2 was confirmed by IR spectroscopy. Results are given in Table 1.

The empirical formula obtained for badakhshanite-(Y), based on 24 O *apfu*, using EDS data is $[Y_{1.62}(Yb_{0.49}Lu_{0.12}Er_{0.08}Dy_{0.06}Tm_{0.03}Ho_{0.02}Gd_{0.01}Sm_{0.01}Tb_{0.01})_{\Sigma 0.83}Th_{0.01}]_{\Sigma 2.46}(Mn_{3.13}Ca_{0.10}Fe^{2+}_{0.09}Mg_{0.02})_{\Sigma 3.34}(Al_{0.73}Sc_{0.30})_{\Sigma 1.03}[(Si_{2.13}B_{6.68}Be_{1.20})_{\Sigma 10.01}O_{24}] = (Y_{1.33}\mathit{REE}_{0.67})_{\Sigma 2}(Mn_{3.13}Y_{0.29}\mathit{REE}_{0.17}Ca_{0.10}Fe^{2+}_{0.09}Mg_{0.02})_{\Sigma 3.80}(Al_{0.73}Sc_{0.30})_{\Sigma 1.03}[(Si_{2.13}B_{6.68}Be_{1.20})_{\Sigma 10.01}O_{24}]$, where $\mathit{REE}_{total} = [(Yb_{0.49}Lu_{0.12}Gd_{0.10}Er_{0.08}Tm_{0.03}Ho_{0.02}Sm_{0.01}Tb_{0.01})_{\Sigma 0.86}Th_{0.01}]_{\Sigma 0.87}$ and that obtained from WDS analyses is $[Y_{1.55}(Yb_{0.47}Lu_{0.12}Dy_{0.04}Er_{0.07}Tm_{0.03}Ho_{0.01}Gd_{0.02}Sm_{0.01}Tb_{0.01})_{\Sigma 0.78}Th_{0.01}]_{\Sigma 2.34}(Mn_{3.47}Ca_{0.11}Fe^{2+}_{0.14})_{\Sigma 3.72}(Al_{0.63}Sc_{0.24})_{\Sigma 0.87}[(Si_{2.10}B_{6.69}Be_{1.20})_{\Sigma 9.99}O_{24}] = (Y_{1.21}\mathit{REE}_{0.78}Th_{0.01})_{\Sigma 2}(Mn_{3.47}Y_{0.34}Ca_{0.11}Fe^{2+}_{0.08})_{\Sigma 4.00}(Al_{0.63}Sc_{0.24}Fe^{2+}_{0.06}\square_{0.07})_{\Sigma 1.00}[(Si_{2.10}B_{6.69}Be_{1.20})_{\Sigma 9.99}O_{24}]$, where $\mathit{REE} = (Yb_{0.47}Lu_{0.12}Dy_{0.04}Er_{0.07}Tm_{0.03}Ho_{0.01}Gd_{0.02}Sm_{0.01}Tb_{0.01})_{\Sigma 0.78}$. In both formulae, Be is from SIMS and B from SIMS and ICP-OES. The ideal formula is $Y_2Mn_4Al(Si_2B_7BeO_{24})$, which requires Y_2O_3 23.80, MnO 29.87, Al_2O_3 5.35, SiO_2 12.67, B_2O_3 25.68, BeO 2.63, total 100.00 wt.%. The Gladstone-Dale compatibility index is $1 - (K_p/K_c) = -0.027$ (excellent).

X-RAY DIFFRACTION DATA

Powder X-ray diffraction data for badakhshanite-(Y) were collected with an RKU-86 camera using Fe$K\alpha$ radiation, a Mn filter, and Ge as an internal standard. The powder data are summarized in Table 2. Unit-cell parameters refined from powder data are $a =$ 12.858(5) Å, $b =$ 4.5803 (7) Å, $c =$ 12.884(4) Å, $V =$ 758.8(6) Å^3. The calculated pattern produced from coordinates and occupancies of the structure refinement for Debye-Scherrer geometry and Fe$K\alpha$ X-radiation was generated using VESTA 3.0 (Momma & Izumi 2011). The 11 strongest lines are shown in bold in Table 2.

TABLE 1. COMPOSITIONAL DATA FOR BADAKHSHANITE-(Y)

EDS Constituent	wt.%	12 Points Range	WDS wt.%	6 Points Range
SiO_2	12.15	11.41–12.8	11.96	11.67–12.08
ThO_2	0.23	0–0.65	0.12	0.10–0.15
UO_2	b.d.l.		b.d.l.	
TiO_2	b.d.l.		b.d.l.	
Sm_2O_3	0.16	0–0.75	0.17	0.11–0.22
Gd_2O_3	0.17	0–0.9	0.30	0.17–0.38
Tb_2O_3	0.11	0–0.52	0.10	0.06–0.15
Dy_2O_3	1.10	0–1.67	0.73	0.56–0.88
Ho_2O_3	0.38	0–1.22	0.19	0.14–0.32
Er_2O_3	1.47	0–2.23	1.34	1.27–1.49
Tm_2O_3	0.52	0–1.11	0.54	0.50–0.60
Yb_2O_3	9.19	7.61–10.02	8.82	8.03–10.52
Lu_2O_3	2.15	1.15–3	2.32	2.12–2.65
Y_2O_3	17.08	15.45–18.1	16.60	15.24–17.33
Sc_2O_3	1.93	1.48–2.25	1.57	1.08–1.96
Al_2O_3	3.52	2.06–4.88	3.06	2.35–3.54
B_2O_3	22.06*	20.90–22.86***	22.06	20.90–22.86***
FeO	0.60	0.26–0.92	0.94	0.33–3.34
MnO	21.09	20.51–21.83	23.33	22.75–23.66
CaO	0.53	0.3–0.71	0.58	0.48–0.69
MgO	0.07	0–0.61	0.00	0–0.01
BeO**	2.84	2.80–2.91	2.84	2.80–2.91
Na_2O	b.d.l.		b.d.l.	
Total	97.35	97.08–101.45	97.57	97.17–97.89

Notes: b.d.l. = below detection limits; * WDS mode, ** SIMS data; *** including SIMS and ICP-OES data.

Single-crystal X-ray diffraction study of badakhshanite-(Y) was done using an Xcalibur - Oxford Diffraction diffractometer equipped with a Sapphire2 CCD detector, graphite monochromatized Mo$K\alpha$ radiation, multilayer optics, and operated at 50 kV and 30 mA. All the tested crystals were twinned, showing pseudotetragonal symmetry as in perettiite-(Y) (Danisi *et al.* 2015). A twinned crystal [twin matrix $00\bar{1}, 0\bar{1}0, \bar{1}00$; twin fraction 0:523(2):0.477(2)], with dimensions $0.11 \times 0.15 \times 0.21$ mm, was chosen for the collection of X-ray diffraction data. Refined unit-cell parameters in orthorhombic symmetry (space group *Pnma*) are a = 12.852(1) Å, b = 4.5848 (5), Å, c = 12.8539(8) Å, $V = 757.38(7)$ Å^3, $Z = 2$. We started with the atom coordinates of perettiite-(Y) (Danisi *et al.* 2015). The crystal structure of badakhshanite-(Y) was refined using SHELXL (Sheldrick 2008) to $R_1 = 0.0431$ on the basis of 1431 unique reflections [$F > 4\sigma F$]. Neutral scattering curves were used (Wilson 1992). The occupancy of the *M*(1) site, showing the highest electron-density in the structure, which was considered a Y-dominant site, was refined with Y and Yb scattering factors, refining their relative proportion with the constraint of summing to a total of 1. The scattering at the *M*(2) and *M*(3) sites, considered as Mn- and Al-dominant sites, were refined with Mn and Fe and Al and Sc scattering factors, respectively. There are three tetrahedrally coordinated sites: *Si*, which was refined with fixed Si occupancy; *B*(1) and *B*(2) [corresponding to the *B*(2) and *B*(3) sites of Danisi *et al.* (2015)], refined with fixed B occupancy; and *T* [corresponding to the *B*(4) site of Danisi *et al.* (2015)], which shows lower scattering and larger size than that expected for a B-centered tetrahedron. In agreement with the Be determination from SIMS, the occupancy at this site was refined with B and Be scattering curves. Data collection, refinement, and unit-cell parameters are given in Table 3. Atom coordinates, site occupancies, and equivalent isotropic-displacement parameters are listed in Table 4. Anisotropic-displacement parameters and table of structure factors and CIF may be obtained from The Depository of Unpublished Data on the MAC website [documents badakhshanite-(Y) CM58, 20-00003][1]. Selected interatomic distances for badakhshanite-(Y) are reported in Table 5. Table 6 lists

---

[1] Supplementary Data are available from the Depository of Unpublished Data on the MAC website (http://mineralogicalassociation.ca/), document "Badakhshanite-(Y), CM58, 20-0003".

TABLE 2. X-RAY POWDER-DIFFRACTION DATA FOR BADAKHSHANITE-(Y)

I_{obs}	d_{obs} (Å)	I_{calc}	d_{calc} (Å)	*hkl*
45	**9.07**	**32.8**	**9.088**	**101**
21	6.43	11.7	6.427	002
42	**4.59**	**37.1**	**4.585**	**010**
39	**4.07**	**12.2**	**4.065**	**103**
		24.4	**4.064**	**301**
14	3.737	9.3	3.732	012
		6.8	3.372	210
4	3.573	2.4	3.584	211
12	3.221	2.8	3.227	212
		5.2	3.213	004
		6.2	3.213	400
100	**3.042**	**100.0**	**3.042**	**113**
		50.0	**3.042**	**311**
		34.4	3.029	303
		3.2	2.874	204
		4.0	2.874	402
		1.6	2.814	312
		48.0	2.631	014
68	**2.637**	**64.5**	**2.631**	**410**
60	**2.533**	**89.8**	**2.528**	**313**
4	2.440	0.6	2.435	214
		7.6	2.292	020
12	2.281	12.9	2.272	404
6	2.221	3.3	2.223	121
		3.9	2.204	503
15	2.146	10.0	2.142	006
		8.9	2.142	600
		5.7	2.129	221
32	**2.119**	**18.3**	**2.117**	**215**
		20.8	2.117	512
10	2.036	10.9	2.036	414
13	1.996	8.2	1.997	123
		6.5	1.997	321
15	1.943	11.6	1.941	016
		10.9	1.941	610
		2.4	1.919	611
21	1.867	11.9	1.866	024
		14.9	1.866	420
36	**1.828**	**52.6**	**1.828**	**323**
		11.2	1.818	107
8	1.786	6.7	1.782	406
24	1.691	1.5	1.690	117
		15.8	1.688	307
		16.4	1.688	703
14	1.662	9.4	1.661	416
		8.2	1.661	614
14	1.614	13.4	1.614	424
		7.4	1.606	800
		5.4	1.589	523
25	1.586	21.2	1.584	317
		18.8	1.584	713
12	1.568	12.2	1.565	026
		9.9	1.565	620
3	1.554	0.4	1.554	621
7	1.526	7.3	1.528	030
		6.1	1.515	606
		2.0	1.438	616
8	1.429	3.9	1.430	133
		4.0	1.430	331
		2.6	1.407	624
10	1.382	6.3	1.380	034
		7.1	1.380	430
		4.7	1.371	814
11	1.364	10.0	1.364	333

Note: the most intense X-ray lines are highlighted in bold.

comparative data for badakhshanite-(Y) and perettiite-(Y).

CRYSTAL STRUCTURE

Badakhshanite-(Y) is a tetrahedral sheet-structure mineral. In the structure there are two [8]-coordinated sites: the Y-dominant *M*(1) site, with subordinate REE^{3+} and <M(1)–O> = 2.346 Å, and the Mn-dominant *M*(2) site, with subordinate Y, *REE*, minor Ca, and Fe^{2+}, and with <M(2)–O> = 2.356 Å (Tables 5 and 7). The *M*(1,2) sites ideally give Y_2Mn_4 *apfu*. An octahedrally coordinated *M*(3) site is occupied by $(Al_{0.73}Sc_{0.27})$ *apfu*, with <M(3)–O> = 1.987 Å; the *M*(3) site ideally gives Al *apfu*. The M(1,2,3) polyhedra form a layer between sheets of tetrahedra having composition $(Si_2B_7BeO_{24})$ (Fig. 6 a–c). Within the sheet of tetrahedra, there are four tetrahedrally coordinated sites: the *Si* site, which is occupied solely by Si, with <Si–O> = 1.623 Å, and gives Si_2 *apfu*; the *B*(1) and *B*(2) sites, which are occupied solely by B, with <B(1)–O> = 1.485 and <B(2)–O> = 1.479 Å, and give B_6 *apfu*; and the *T* site, which is occupied by $(Be_{1.20}B_{0.80})$ *apfu*, ideally (BeB) *apfu*, with <*T*–O> of 1.557 Å (Tables 5 and 6). Cations for the *T* site (available from the chemical analysis) are $B_{0.69}Be_{1.20}Si_{0.10}$ (Table 1). We assume that the determination by SIMS of a larger quantity of B ($B_{6.68}$ *apfu*) is more reliable than that of a smaller quantity of Be ($Be_{1.20}$ *apfu*). Hence a site occupancy of $B_{0.68}$ (3.4 *epfu*) was fixed at the *B*(4) site during the refinement and the site

TABLE 3. DATA COLLECTION, REFINEMENT, AND UNIT-CELL PARAMETERS FOR BADAKHSHANITE-(Y)

Temperature	293(2) K
Wavelength	0.71073 Å
Crystal system	Tetragonal
Space group	*Pmna*
Unit cell dimensions (Å)	a = 12.8518(10) b = 4.5848(5) c = 12.8539(8)
Volume (Å^3)	757.39(11)
Z	2
Density (calculated)	4.363 g/cm^3
Absorption coefficient	12.61 mm^{-1}
F(000)	937
Crystal size	0.21 × 0.15 × 0.11 mm^3
θ-range for data collection	3.17 to 36.04°
Index ranges	$-21 \leq h \leq 21$, $-6 \leq k \leq 6$, $-20 \leq l \leq 20$
Reflections collected	20579
Independent reflections	1431 [$R_{(int)}$ = 0.115]
Refinement method	Full-matrix least-squares on F^2
Data / restraints / parameters	1431 / 0 / 110
Goodness-of-fit on F^2	0.987
Final R indices [$I > 2\sigma I$]	$R1$ = 0.0431, wR2 = 0.1018
R indices (all data)	$R1$ = 0.0568, wR2 = 0.1084
Extinction coefficient	0.0002(6)
Largest diff. peak and hole	4.543 and –3.941 e·Å^{-3}

TABLE 5. INTERATOMIC DISTANCES FOR BADAKHSHANITE-(Y)

M(1)–O(3)^a ×2	2.275(3)	Si–O(3)^d	1.586(6)
M(1)–O(7) ×2	2.361(4)	Si–O(6) ×2	1.631(4)
M(1)–O(2)^b ×2	2.362(4)	Si–O(5)	1.646(5)
M(1)–O(6)^c ×2	2.384(4)	<Si–O>	1.623
<M(1)–O>	2.346		
		B(1)–O(2)^c	1.407(7)
M(2)–O(8)^e	2.211(4)	B(1)–O(8)^g	1.484(7)
M(2)–O(4)	2.242(4)	B(1)–O(7)	1.501(7)
M(2)–O(2)^c	2.269(4)	B(1)–O(6)^c	1.547(7)
M(2)–O(2)	2.300(4)	<B(1)–O>	1.485
M(2)–O(1)^f	2.303(4)		
M(2)–O(5)	2.322(3)	B(2)–O(7) ×2	1.473(6)
M(2)–O(7)	2.545(4)	B(2)–O(4) ×2	1.484(6)
M(2)–O(6)	2.652(4)	<B(2)–O>	1.479
<M(2)–O>	2.356		
		T–O(1)	1.478(11)
M(3)–O(1) ×2	1.941(5)	T–O(5)^h	1.579(12)
M(3)–O(4) ×4	2.054(4)	T–O(4)^h ×2	1.585(7)
<M(3)–O>	2.016	<T–O>	1.557

Symmetry operators: a: $-x+1, -y+1, -z+1$; b: $-x+{}^1/_2, y+1, z+{}^1/_2$; c: $-x+1, y, -z+{}^1/_2$; d: $x-{}^1/_2, y, -z+{}^1/_2$; e: $-x+{}^1/_2, -y+2, z-{}^1/_2$; f: $-x, -y+2, -z+1$; g: $-x+{}^1/_2, -y+1, z-{}^1/_2$; h: $-x, -y+1, -z+1$.

TABLE 4. ATOM COORDINATES AND EQUIVALENT DISPLACEMENT PARAMETERS (Å^2) FOR BADAKHSHANITE-(Y)

Atom	x	y	z	U^{eq}	BV* (*vu*)
M(1)	0.35577(5)	0	½	0.00558(18)	3.182
M(2)	0.14257(6)	0.97691(16)	0.30203(10)	0.0099(3)	2.079
M(3)	0	1	½	0.0096(10)	3.286
Si	0	0.5280(4)	0.14956(17)	0.0077(4)	4.012
B(1)	0.2892(5)	0.4590(14)	0.3474(5)	0.0083(11)	2.947
B(2)	0.1612(6)	½	½	0.0100(17)	2.969
T	0	0.464(2)	0.6241(8)	0.015(2)	2.662
O(1)	0	0.7857(12)	0.6302(4)	0.0124(12)	1.887
O(2)	0.2046(3)	0.7652(9)	0.1521(3)	0.0089(7)	1.870
O(3)	½	0.7686(13)	0.4391(4)	0.0101(12)	2.047
O(4)	0.0942(3)	0.6883(9)	0.4343(3)	0.0168(9)	1.934
O(5)	0	0.6839(11)	0.2649(4)	0.0118(11)	1.947
O(6)	0.1021(3)	0.3184(9)	0.1405(3)	0.0112(9)	2.074
O(7)	0.2277(3)	0.3180(8)	0.4330(3)	0.0124(8)	2.021
O(8)	¼	0.6759(11)	¾	0.0119(11)	2.090

* BV = Bond valence in valence units (*vu*); values from Gagné & Hawthorne (2015)

TABLE 6. COMPARISON OF BADAKHSHANITE-(Y) AND PERETTIITE-(Y)

Mineral	badakhshanite-(Y)	perettiite-(Y)*
Ideal formula	$Y_2Mn_4Al(Si_2B_7BeO_{24})$	$Y_2Mn_4Fe^{2+}(Si_2B_8O_{24})$
Space group	*Pnma*	*Pnma*
a (Å)	12.852	12.8252
b	4.5848	4.6187
c	12.8239	12.8252
Z	2	2
$D_{calc.}$ (g cm^{-3})	4.41	4.533
$D_{meas.}$ (g cm^{-3})	-	-
Strongest reflections in the X-ray powder diffraction data, *d*/Å (I_{rel})	3.042(100)	3.05(100)
	2.637(68)	2.64(67)
	2.533(60)	2.54(60)
	4.59(42)	4.63(52)
	1.828(36)	1.84(52)
	1.867(21)	1.87(33)
optical class (sign)	biaxial (–)	biaxial
α (590 nm)	1.805	1.82
β	1.823 (calc.)	-
γ	1.835	1.84
$2V_{X(meas)}$ (°)	60	-
$2V_{calc}$ (°)		-

* Data from Danisi *et al.* (2015)

scattering of Be refined to 5.8(5) *epfu* corresponding to 1.45 Be *apfu* (with a total scattering of 9.2 *epfu* at the *T* site). Hence, we assign $Be_{1.20}B_{0.70}Si_{0.10}$ to the *T* site, with a calculated site-scattering of 9.7 *epfu*. All the anion sites in badakhshanite-(Y) are occupied by oxygen, as in perettiite-(Y).

The crystal in Figure 4 has a thin rim, enriched in Fe and Mn and depleted in Y, that can be related to a heterovalent substitution at the *M*(2) site. As the excess charge brought by Y at the *M*(2) site is compensated by an excess of Be at the *T* site in the studied sample, the substitution $^{M(2)}Y^{3+} + {}^{T}Be^{2+} \leftrightarrow {}^{M(2)}Mn^{2+}(Fe^{2+}) + {}^{T}B^{3+}$ is limited but can also be operative, leading to another hypothetical endmember $Y_2(Mn_3Y)Al(Si_2B_6Be_2O_{24})$.

Tetrahedral sheet topology

The sheet is parallel to (010), and *Si*, *B*(1,2), and *T* tetrahedra form four-, five-, and eight-membered rings (Fig. 6) in the ratio 1:1:3. Using a net representation, a

TABLE 7. REFINED SITE-SCATTERING AND ASSIGNED SITE POPULATIONS FOR BADAKHSHANITE-(Y)

Site	Refined site-scattering (*epfu*)	Assigned site population (*apfu*)	Calculated site-scattering (*epfu*)	<Ct–O>$_{obs.}$ * (Å)	Ideal composition (*apfu*)
$^{[8]}M(1)$**	92.9(6)	$Y_{1.21}REE_{0.79}$	102.20	2.346	Y_2
$^{[8]}M(2)$	102(14)	$Mn_{3.47}Y_{0.34}Ca_{0.11}Fe^{2+}{}_{0.08}$	104.29	2.356	Mn_4
$^{[6]}M(3)$	14.3(4)	$Al_{0.63}Sc_{0.24}Fe^{2+}{}_{0.06}\square_{0.07}$	14.79	1.987	Al
$^{[4]}Si$	28	Si_2	28	1.623	Si_2
$^{[4]}B(1)$	20	B_4	20	1.484	B_4
$^{[4]}B(2)$	10	B_2	10	1.478	B_2
$^{[4]}T$	9.2***	$Be_{1.20}B_{0.70}Si_{0.10}$	9.7	1.558	(BeB)

* Ct = cation; ** 0.79 *REE* = $[(Yb_{0.47}Lu_{0.12}Dy_{0.04}Er_{0.07}Tm_{0.03}Ho_{0.01}Gd_{0.02}Sm_{0.01}Tb_{0.01})_{\Sigma 0.78}Th_{0.01}]$; corresponding *f*-curve of 69.63 el.; *** sum of the site-scattering of 5.8(5) *epfu* (Be species) and fixed 3.4 *epfu* corresponding to $B_{0.68}$ *apfu* available from the chemical analysis.

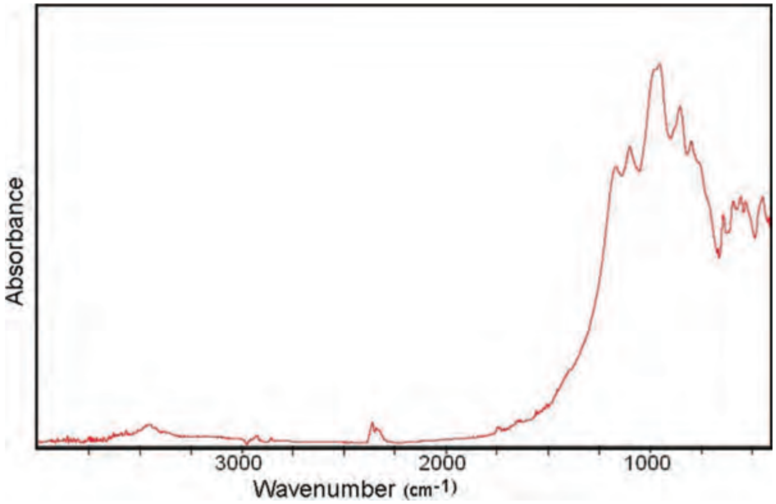

FIG. 5. Badakhshanite-(Y) IR spectrum.

tetrahedron can be considered a vertex. The sheet of tetrahedra in badakhshanite-(Y) can be represented as a net having three types of vertex, two 3-connected and one 4-connected (Hawthorne 2015, Hawthorne *et al*. 2019). These vertices are: (4.5^2), a 3-connected vertex where one four-membered ring and two five-membered rings are incident at the vertex; $(5^2.8)$, a 3-connected vertex where two five-membered rings and one eight-membered ring are incident at the vertex; and (4.5.8.5), a 4-connected vertex where one four-membered ring, two five-membered rings, and one eight-membered ring are incident at the vertex (Fig. 7a). We count a total of 5 vertices per 2D unit-cell (with four layers in one unit-cell), with this configuration forming a $[(4.5^2)_1(4.5.8.5)_1(5^2.8)_3]_4$ net. Regarding the orientation of the tetrahedra, we can consider the orientation of the apical anion as up (u) or down (d) or neither (o). Therefore, a string can be used to describe the polarity of tetrahedra within the rings in the sheet. In this case, it is (uodo)(u^2odo)(uod^2o)(uouododo), meaning that the two five-membered rings are oriented alternately within the layer. This type of sheet is present in the structures of semenovite-(Ce) (Mazzi *et al*. 1979), harstigite (Hesse & Stümpel 1986), and perettiite-(Y) (Danisi *et al*. 2015). In semenovite-(Ce) (Fig. 7c), the 4-connected tetrahedra are occupied by Si^{4+} and Be^{2+}. In harstigite (Fig. 7e), the 4-connected tetrahedron and one 3-connected tetrahedron are occupied by Be^{2+} and the remaining 3-connected tetrahedra are occupied by Si^{4+}. In perettiite-(Y), one 3-connected tetrahedron is occupied by Si^{4+} and the remaining 3- and 4-connected tetrahedra are occupied by B^{3+}; one 3-connected tetrahedron is partly occupied by Be^{2+}, and this tetrahedron corresponds to the 3-connected tetrahedron occupied by Be^{2+} in harstigite (Fig. 7e).

Interstitial sheet topology

The interstitial complex in badakhshanite-(Y) consists of two Y^{3+} ions coordinated by eight O^{2-}, four Mn^{2+} ions coordinated by eight O^{2-}, and an Fe^{2+} ion coordinated by six O^{2-}. In perettiite-(Y), the last is Al. The interstitial complex in semenovite-(Ce) consists of one Ce^{3+} ion coordinated by eight O^{2-}; two Na^+ ions, one coordinated by six O^{2-}, one F^-, and one $(OH)^-$ and another coordinated by four O^{2-}, two F^-, and two $(OH)^-$; one Ca^{2+} ion (with minor Na^+ substitution) coordinated by seven O^{2-} and one F^-; and two Fe^{2+} ions, one coordinated by six O^{2-} and another coordinated by four O^{2-} and two $(OH)^-$. The interstitial complex in harstigite consists of three Ca^{2+} ions coordinated by seven O^{2-} and one $(OH)^-$, by seven O^{2-}, and by seven O^{2-} and $(OH)^-$, and one Mn^{2+} ion coordinated by six O^{2-}.

ORIGIN OF THE MINERAL

Badakhshanite-(Y) is found in the near-miarolitic pegmatite complex in association with quartz, spessartine, schorl, and tusionite. Apparently, the formation time of the near-miarolitic complex coincides with the formation of miaroles in the granite pegmatite. Badakhshanite-(Y) often occurs as well-formed idiomorphic crystals, frequently inter-

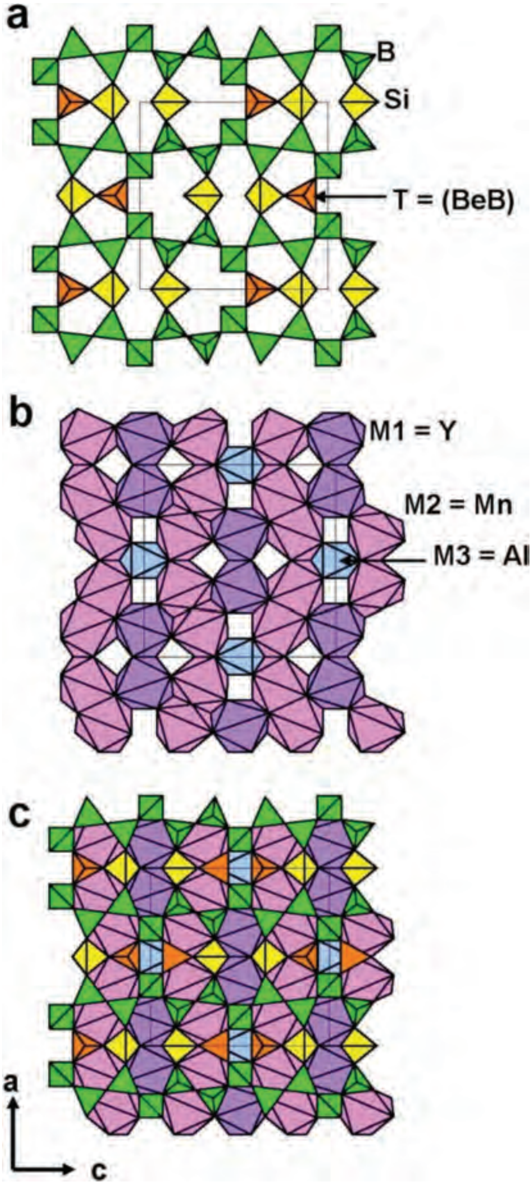

FIG. 6. The crystal structure of badakhshanite-(Y). (a) The ($Si_2B_7BeO_{24}$) sheet at $y = 0.5$. (b) The layer of the [8]-coordinated Y-dominant M(1) polyhedra, [8]-coordinated Mn-dominant M(2) polyhedra, and Al-dominant M(3) octahedra at $y = 0$. (c) The ($Si_2B_7BeO_{24}$) sheet superimposed on the layer of M(1–3) polyhedra. SiO_4 tetrahedra are yellow, BO_4 tetrahedra are green, TO_4 tetrahedra of composition (BeB) are orange, and M(1), M(2), and M(3) polyhedra are purple, magenta, and pale blue, respectively.

grown with tusionite, as inclusions in schorl, and seldom in quartz and spessartine. It also occurs as aggregates on curved surfaces of the above-mentioned minerals, which we interpret as surfaces of mutual growth.

Free-standing crystals occur in small cavities and both penetrate and partially overgrow schorl and spessartine.

All this suggests that badakhshanite-(Y) and tusionite began to crystallize earlier than spessartine and schorl and continued to crystallize after the latter ceased crystallization. The paragenesis of badakhshanite-(Y) with tourmaline and tusionite indicates enrichment of the environment with boron. According to experimental data, tusionite can crystallize only at high boron concentrations in solution (B_2O_3 9–14 wt.%) and at strongly reducing conditions (Diman & Nekrasov 1965, Nekrasov 1976). High-boric acidic or slightly acidic solutions are also favorable for tourmaline crystallization (Peretyazhko *et al*. 2000). The discovery of sassolite ($B(OH)_3$) in fluid inclusions in minerals of neighboring pegmatite veins of the Kukurt pegmatite field is indirect confirmation of the role of highly concentrated fluids highly enriched in boron during formation of miaroles and near-miarolitic complexes (Smirnov *et al*. 2000). Many badakhshanite-(Y) crystals show skeletal growth (Fig. 3), which may be due to an increased viscosity of the mineral-forming environment or a high rate of crystal growth. It is possible that colloidal aqueous silicate fluids were the crystallization medium of the paragenetic association involving badakhshanite-(Y) (Smirnov 2015), possibly intermediate or final products of the gradual transformation of magmatic melt into aqueous fluids.

ACKNOWLEDGMENTS

We thank A.A. Agakhanov, F.K. Rakhimi, R.D. Bakhtdavlatov, I. Oymukhammadzoda, R.U. Sabirova, A.R. Fayziyev, S. Makhmadsharif, N. Safaraliyev, F. Malakhov, and S. Elnazarov for help with the field work, and P.Yu. Plechov, H.J. Sherov, S.G Simakin, and N.V. Chukanov for help with the experimental work. We thank reviewers Thomas Armbruster and Federica Zaccarini and Associate Editor Jim Evans. FC acknowledges financial support by the grant Ricerca Locale 2014, Università di Milano and from the Italian Ministry of Education (MIUR) through the project "Dipartimenti di Eccellenza 2018–2022"; this work was supported by a Discovery grant from the Natural Sciences and Engineering Research Council of Canada to FCH.

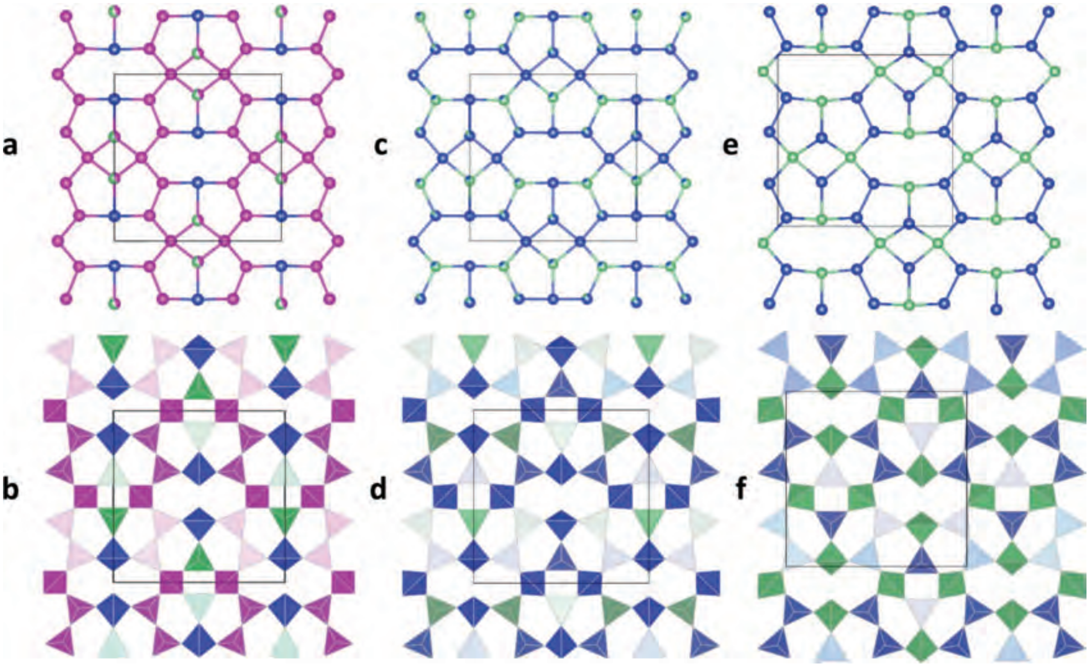

FIG. 7. The $[(4.5^2)_1(4.5.8.5)_1(5^2.8)_3]_4$ net and corresponding sheets of tetrahedra in (a, b) badakhshanite-(Y); (c, d) semenovite-(Ce); and (e, f) harstigite.

REFERENCES

DANISI, R.M., ARMBRUSTER, T., LIBOWITZKY, E., WANG, H.A.O., GÜNTHER, D., NAGASHIMA, M., REUSSER, D., & BIERI, W. (2015) Perettiite-(Y), $Y^{3+}{}_2Mn^{2+}{}_4Fe^{2+}[Si_2B_8O_{24}]$, a new mineral from Momeik, Myanmar. *European Journal of Mineralogy* **27**, 793–803.

DIMAN, E.N. & NEKRASOV, I.YA. (1965) Hydrothermal synthesis of nordenskioldite and its analogues. *Doklady Akademii Nauk SSSR* **164(4)**, 89–897 (in Russian).

DMITRIEV, E.A. (1983) Granite pegmatites of Eastern Pamir and specific of their gemstone mineralization. *Izvestya Academii Nauk Tadzhikskoi SSR. Serya geologicheskih i fiziko- technicheskih nauk* **N3**, 73–81 (in Russian).

DZHURAYEV, Z.T., ZOLOTAREV, A.A., PEKOV, I.V., & FROLOVA, L.V. (1998) Hambergite from pegmatite veins of the Eastern Pamir. *Proceedings of the Russian Mineralogical Society* **127(4)**, 132–139 (in Russian with English abstract).

GAGNÉ, O.C. & HAWTHORNE, F.C. (2015) Comprehensive derivation of bond-valence parameters for ion pairs involving oxygen. *Acta Crystallographica* **B71**, 562–578.

HAWTHORNE, F.C. (2015) Generating functions for stoichiometry and structure of single- and double-layer sheet-silicates. *Mineralogical Magazine* **79**, 1675–1709.

HAWTHORNE, F.C., UVAROVA, Y.A., & SOKOLOVA, E. (2019) A structure hierarchy for silicate minerals: Sheet silicates. *Mineralogical Magazine* **83**, 3–55.

HESSE, K.F. & STÜMPEL, G. (1986) Crystal structure of harstigite, $MnCa_6Be_4[SiO_4]_2[Si_2O_7]_2(OH)_2$. *Zeitschrift für Kristallographie - Crystalline Materials* **177**, 143–148.

MAZZI, F., UNGARETTI, L., DAL NEGRO, A., PETERSON, O.V., & RØNSBO, J.G. (1979) The crystal structure of semenovite. *American Mineralogist* **64**, 202–210.

MIRAKOV, M.A., PAUTOV, L.A., SHODIBEKOV, M.A., FAIZIEV, A.R., & KHVOROV, P.V. (2018a) Scandium-bearing spessartine from pegmatites of the Kukurt pegmatite field (the Eastern Pamir). *Reports of the Academy of Sciences of the Republic of Tajikistan* **61(5)**, 491–493 (in Russian with English abstract).

MIRAKOV, M.A., PAUTOV, L.A., SHODIBEKOV, M.A., PLECHOV, P.YU., & KARPENKO, V.YU. (2018b) A new scandium-bearing variety of tusionite from the Eastern Pamir. *Proceedings of the Russian Mineralogical Society* **147(4)**, 84–96 (in Russian with English abstract).

MOMMA, K. & IZUMI, F. (2011) *VESTA 3* for three-dimensional visualization of crystal, volumetric and morphology data. *Journal of Applied Crystallography* **44**, 1272–1276.

Nekrasov, I.Ya. (1976) *A phase relations in a tin-bearing systems*. Nauka, Moscow, Russia, 362 pp. (in Russian).

Peretyazhko, I.S., Prokofiev, V.Y., Zagorsky, V.E., & Smirnov, S.Z. (2000) Role of boric acids in the formation of pegmatite and hydrothermal minerals: Petrologic consequences of sassolite (H_3BO_3) discovery in fluid inclusions. *Petrology* **8(3)**, 214–237.

Pouchou, J.L. & Pichoir, F. (1985) 'PAP' φ(ρZ) procedure for improved quantitative microanalysis. *In* Microbeam Analysis (J.T. Armstrong, ed.). San Francisco Press, San Francisco, California, Untied States (104–106).

Rossovsky, L.N., Morozov, S.A., & Skrigitil', A.M. (1991) Features of formation of myarolic pegmatites of Eastern Pamir. *Izvestya Academii Nauk SSSR* **N5**, 92–103 (in Russian).

Sheldrick, G.M. (2008) A short history of *SHELX*. *Acta Crystallographica* **A64**, 112–122.

Skrigitil', A.M. (1996) Gemstones in pegmatites of Eastern Pamir. *Mir kamnya (World of stones)* **N11**, 11–17.

Smirnov, S.Z. (2015) The fluid regime of crystallization of water-saturated granitic and pegmatitic magmas: A physicochemical analysis. *Russian Geology and Geophysics* **56(9)**, 1292–1307.

Smirnov, S.Z., Peretyazhko, I.S., Prokofiev, V.Yu., Zagorsky, V.E., & Shebanin, A.P. (2000) The first evidence of sassolite (H_3BO_3) in fluid inclusions in minerals. *Russian Geology and Geophysics* **4(2)**, 193–205.

Wilson, A.J.C., Ed. (1992) *International Tables for Crystallography. Volume C: Mathematical, physical and chemical tables*. Kluwer Academic Publishers, Dordrecht, Netherlands.

Zolotarev, A.A. (1996) Gem and collection-worth tourmaline from the Pamirs (crystallomorphology, coloring, crystallochemistry). *Proceedings of the Russian Mineralogical Society* **125(4)**, 32–46 (in Russian with English abstract).

Received January 21, 2020. Revised manuscript accepted March 14, 2020.